Check for updates

RESEARCH ARTICLE

Editor's Choice

ADVANCED MATERIALS TECHNOLOGIES

www.advmattechnol.de

Light Induced Training of 3D Printed Mechanical Metamaterials

David Schwarz, Johan Liotier, Viacheslav Slesarenko,* and Jürgen Rühe*

Stimuli-responsive materials often react to changes in environmental conditions by altering their shape. Here, it is shown that even changes in materials that are not directly observable, such as local stiffening, can be exploited to introduce the concept of trainable materials. A fully 3D-printable filament based on thermoplastic polyurethane (TPU) functionalized with a bivalent crosslinker capable of undergoing a C,H insertion reaction under UV irradiation was developed. Specimens printed from this filament demonstrate a gradual increase in stiffness, reaching almost 300% of their initial stiffness after 50 hours of irradiation. To exploit this tunability, mechanical metamaterials incorporating the developed material are engineered. By utilizing an instability-driven transformation under compression, it is demonstrated how local stiffening can be amplified through rational design. Moreover, by exploiting the unusual mechanical behavior of metamaterials arising from their internal architecture, a closed-loop system is presented in which, under compressive load, the metamaterial closes an electric circuit that activates UV light, which in turn modifies the properties of the base material. Through this approach, two trainable systems are realized: one that progressively conforms its shape to mechanical compression, and another that gradually increases its resistance to an applied force, mimicking the physical training of biological tissues.

1. Introduction

Nature offers a wide variety of examples of adaptation: upon repeated stimuli, muscles grow,[1] bones become stronger,[2,3] and leaf petioles change shape.[4] In engineering practice, we still often rely on materials with persistent properties, which is reasonable for many applications. At the same time, materials such as shape memory alloys,[5,6] polymers,[7,8] liquid crystal elastomers,[9,10] and hydrogels[11,12] alter their shape and behavior in response to temperature,[13] humidity,[14] or pH.[15] This allows their use as components of larger systems, usually as actuators. Materials may also undergo changes that do not directly manifest as a change in shape, for example, through color variation in self-reporting systems[16–18] or through stiffening.[19–21] The ability to store or even accumulate such changes is associated with the phenomenon of memory, which has been conceptually realized and observed on both the material[22] and structural level.[23] If changes in mechanical properties (e.g., stiffening) are not accompanied by a shape change, they can still be revealed under specific conditions, for example, when an external load is applied. Noticeably, even small variations can be amplified if the structure is rationally designed, as in the case of mechanical metamaterials.

Mechanical metamaterials are often defined as materials with rationally and purposefully designed internal architectures that give rise to a desired set of unorthodox mechanical properties.[24] Such architectures enable the realization of metamaterials that exhibit negative effective stiffness,[25] close-to-zero shear modulus,[26] or coupling between different deformation modes.[27,28] Among the most common manifestations of these unusual properties is a negative Poisson's ratio in so-called auxetic metamaterials.[29] Auxetic behavior can be found in some biological materials,[30] but more often it is engineered in artificial metamaterials via the rational design of the elementary building block, the unit cell, which periodically repeats throughout the metamaterial.[31] Within the unit cell, intricate connections of beams allow the engineering of the material's overall response to mechanical load. Elegantly, this design is geometric and therefore less sensitive to the unit cell's dimensions and base material. Hence, their functionality can be achieved over multiple length scales and base materials, ranging from nano- and micrometers[27,32,33] for micro-electromechanical systems (MEMS) to meters[34] for seismic shields. By further

D. Schwarz, J. Liotier, V. Slesarenko, J. Rühe
Cluster of Excellence livMatS@FIT - Freiburg Center for Interactive Materials and Bioinspired Technologies
University of Freiburg
79110 Freiburg, Germany
E-mail: johan.liotier@livmats.uni-freiburg.de; viacheslav.slesarenko@livmats.uni-freiburg.de

J. Liotier, J. Rühe
Department of Microsystems Engineering (IMTEK)
Laboratory for Chemistry and Physics of Interfaces
Albert-Ludwigs-Universität Freiburg
79110 Freiburg, Germany

The ORCID identification number(s) for the author(s) of this article can be found under https://doi.org/10.1002/admt.202501416

© 2025 The Author(s). Advanced Materials Technologies published by Wiley-VCH GmbH. This is an open access article under the terms of the Creative Commons Attribution License, which permits use, distribution and reproduction in any medium, provided the original work is properly cited.

DOI: 10.1002/admt.202501416

23657709x, 2025, 23, Downloaded from https://advanced.onlinelibrary.wiley.com/doi/10.1002/admt.202501416 by Viacheslav Slesarenko - Albert-Ludwigs-Universitat , Wiley Online Library on [04/11/2026]. See the Terms and Conditions (https://onlinelibrary.wiley.com/terms-and-conditions) on Wiley Online Library for rules of use; OA articles are governed by the applicable Creative Commons License

modifying the internal connections within the unit cell, more advanced functionalities such as logic gates or memory[23,35] are achievable. By carefully designing the elements to allow for self-contact, switching the sign of Poisson's ratio during deformation seems possible. For instance, initially auxetic metamaterials can, upon sufficient compression, expand beyond their initial width.[36] At the same time, even such complex mechanical responses are fixed at the design stage and normally cannot be changed after fabrication. To add new functionalities and enable changes in the mechanical behavior of already fabricated metamaterials, stimuli-responsive materials can be integrated into the metamaterial architecture.[37]

There are several possible approaches that can add stimuli sensitivity to existing polymers. Among them, C,H insertion crosslinking (CHic) is a chemical strategy to achieve a crosslinked polymer network. With this method, it is possible to crosslink polymers without catalysis in the solid state using only heat or UV-irradiation.[38–42] Upon triggering, reactive moieties are activated and react with neighboring C–H bonds to create crosslink points. The resulting covalent C–C bonds create a strongly bonded network. In addition, the reaction is non-specific, allowing to be used regardless of the polymer backbones and even to link additives in the network such as fluorescent dyes or biological molecules.[43] After crosslinking, the properties of the material changes drastically, notably regarding mechanical properties, solvent resistance and heat resistance.[44,45] These moieties are usually incorporated into the desired precursor polymer by copolymerization with the desired comonomer, thus limiting polymer usage. To avoid that, we recently developed a bivalent crosslinker able to be inserted into the polymer chain post polymerization.[46] This methodology is interesting as it does not require to know the exact structure of the polymer, only C–H bonds must be present, a requirement fulfilled for practically any polymer. This method allows the use of commercial polymers and to an extent also commercial 3D printable materials.

Being able to treat commercially available 3D printable materials opens new possibilities. Treating a commercial filament allows to easily obtain large amounts of polymer, omitting elaborate synthesis. Indeed, the necessary amount of crosslinker needed to obtain a then crosslinkable material is comparatively low, thus reducing the synthetic effort needed.[46] Here we set out to introduce CHic chemistry into a 3D printed structure to achieve a novel, trainable material system. The main goal is to exploit the ability of a CHic-treated polymer to change its stiffness upon UV irradiation and to transform such changes into unconventional, trainable behavior through the rational architecture of a mechanical metamaterial (**Figure 1**). The realization of a metamaterial capable of accumulating information about previous mechanical and non-mechanical stimuli and changing its behavior accordingly can open new approaches in emerging fields such as soft robotics.

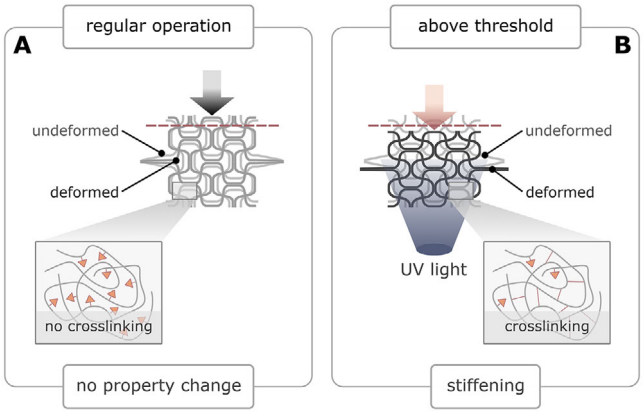


Figure 1. Schematic of the trainable material system utilizing the properties of the mechanical metamaterial and UV crosslinking. A) The metamaterial does not pass the threshold during loading, therefore no changes in mechanical properties happen. B) The metamaterial is loaded above threshold, therefore a UV light is triggered and crosslinking of the base-material is induced. The metamaterial itself becomes stiffer.

2. Results and Discussion

2.1. Material Design

In order to obtain a UV-crosslinkable and printable TPU, it is required to add a UV-reactive unit to the material. This might raise the idea to use an additive mixed into the material. However, this additive could be lost during the printing process due to high shear and elevated temperatures. To avoid that, the UV-reactive unit should be covalently linked to the polymer chain. This idea is derived from our previously published work where we developed a small molecule bearing a diazo compound and a benzophenone unit that can be easily mixed into a polymer.[46] Upon elevated temperature, the diazo compound is converted to a carbene that inserts in the closest neighboring C,H bond, covalently attaching the small molecule to the polymer chain. The second benzophenone part is then untouched and ready to be used to crosslink the polymer using UV-light. This strategy was proven successful with many polymers regardless of their structure and even with polyurethane of unknown chemical structure. The use of benzophenone is good on thin film because of its high reactivity under irradiation at 254 nm. However, while still reactive at 365 nm, its reactivity is slowed significantly. This would make its use on larger objects more difficult as the penetration depth of light at 254 nm is much lower than at 365 nm and typically only some hundred nanometers to a few microns. To avoid that, we decided to develop a new crosslinker, combining a 2-(2-diazo-2-phenylacetoxy) ethyl methacrylate (PEDAz) and an anthraquinone moiety noted PA, using the same concept while substituting the benzophenone unit by an anthraquinone unit. Anthraquinone units exhibit a higher absorption at 365 nm than benzophenone while still being able to undergo C,H insertion crosslinking.[47] The new molecule is obtained in a three-step synthesis (**Figure 2A**). The first step, leading to compound 1, is a Steglich esterification between phenylacetic acid and ethylene glycol. Compound 1 is then coupled to 2-hydroxyanthraquinone through a Mitsunobu reaction yielding compound 2. Finally, PA is obtained by adding a diazo compound through Regitz transfer. The global yield of this 3 step synthesis is 66%, allowing us to easily obtain several grams of the crosslinker.

The material production is described in Figure 2B,C. The TPU filament is insoluble in most solvents, which makes the C,H insertion of the filament more difficult. However, this filament swells strongly in solvents such as dichloromethane (DCM).

 © 2025 The Author(s). Advanced Materials Technologies published by Wiley-VCH GmbH

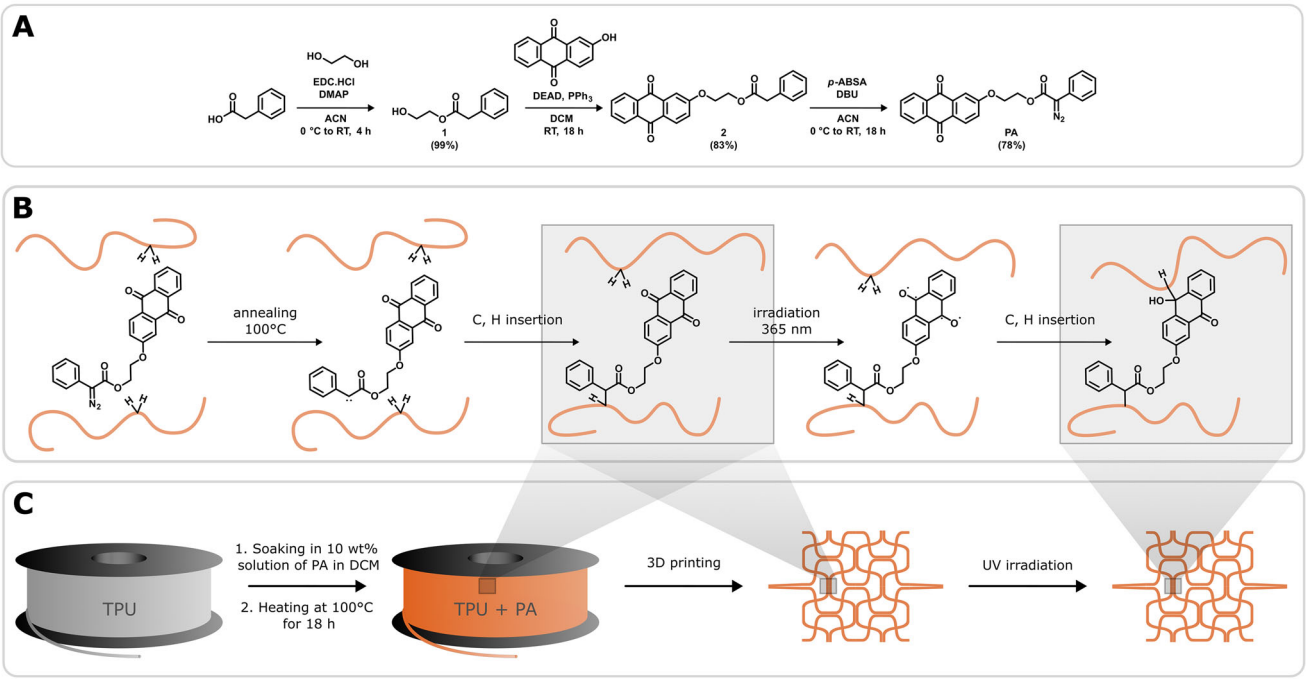


Figure 2. A) Schematic of the synthesis of PA. B) Molecular reaction of PA crosslinker with the polymer chains during the modification of the polymer and the crosslinking. C) Process-schematic of modification and printing of the filament.

Using this property, it is possible to make the PA molecule penetrate the filament. We used a solution of PA in DCM using 10 *wt%* of the crosslinker compared to the polymer. This low crosslinker content was selected to conserve most of the properties of the base-material. Then annealing at 100 °C for 18 h is performed to activate the diazo compound and link the crosslinker to the polymer chain. Using UV-vis measurements of the modified and unmodified filaments, the final crosslinker content is found to be 5 *wt%* (see experimental section). This base-material is then printable using similar parameters compared to the unmodified filament.

2.2. Property Change Induced by UV Irradiation

Crosslinkable PA mixed into TPU filament for fused filament fabrication (FFF) 3D printing enables a UV induced change in properties, which ultimately allows us to design a trainable material system. To assess the base-material's properties, we printed tensile specimens from the new material. These specimens were then exposed to UV light (λ = 365 nm) and we subsequently probed their stiffness. The process was repeated multiple times to reach an accumulated irradiation time of 55.4 h. After an initially steep (1.5×) increase in stiffness over 5 h of irradiation, we subsequently observe a proportional increase in stiffness with irradiation time (**Figure** 3A). Ultimately, a three-fold increase in stiffness was achieved during this process. One might assume, that more irradiation would eventually saturate the number of crosslinks formed as we would activate more crosslinkers until they are consumed completely.[48] Consequently the stiffness will increase and asymptotically reach a maximum value. In contrast, after this irradiation time we rather observe some cracking of the base TPU-material. UV degradation in the form of microcracking in PU and TPU materials is a well-known process.[49,50] However, the proportionality of irradiation and mechanical properties at times up to two days yields a well defined base-material for our trainable material system.

With the prior testing procedure, we obtain the ideal potential crosslinking of the modified TPU. Additionally, we also want to assess the properties with higher time-resolution and make sure stiffening happens solely due to UV-irradiation. Therefore, we tested a tensile-specimen continuously irradiated with custom UV-lamps mounted to the tensile-testing setup. As a control, we repeated the experiment with a not yet irradiated specimen and UV-lights turned off during testing. We can observe the aforementioned stiffening only if the UV-lamps are turned on, as depicted in Figure 3B. It should be noted, that when we use a lower intensity light source and smaller part of the geometry irradiated, we also see a reduced stiffening effect compared with Figure 3A. Boubarki et al.[49] observe an initial drop of stiffness upon irradiation of pure TPU, which is not happening for the PA treated TPU as depicted by the blue curve in Figure 3B. This indicates, that only the conjunction of PA's presence and UV exposure yield significant stiffening.

Additionally, we examine the material's response time to UV irradiation and its stiffness retention after irradiation is turned off. To accomplish this, we used UV-lights during stiffness probing in the tensile testing machine. This enabled us to intermittently turn the light source on or off during tensile-testing as depicted in Figure 3C. Here, we observe an immediate onset of stiffening upon UV irradiation and retention of reached stiffness when lights are off.

© 2025 The Author(s). Advanced Materials Technologies published by Wiley-VCH GmbH

2365709x, 2025, 23, Downloaded from https://advanced.onlinelibrary.wiley.com/doi/10.1002/admt.202501416 by Viacheslav Slesarenko - Albert-Ludwigs-Universitat , Wiley Online Library on [04/11/2026]. See the Terms and Conditions (https://onlinelibrary.wiley.com/terms-and-conditions) on Wiley Online Library for rules of use; OA articles are governed by the applicable Creative Commons License

2365709x, 2025, 23, Downloaded from https://advanced.onlinelibrary.wiley.com/doi/10.1002/admt.202501416 by Viacheslav Slesarenko - Albert-Ludwigs-Universitat , Wiley Online Library on [04/11/2026]. See the Terms and Conditions (https://onlinelibrary.wiley.com/terms-and-conditions) on Wiley Online Library for rules of use; OA articles are governed by the applicable Creative Commons License

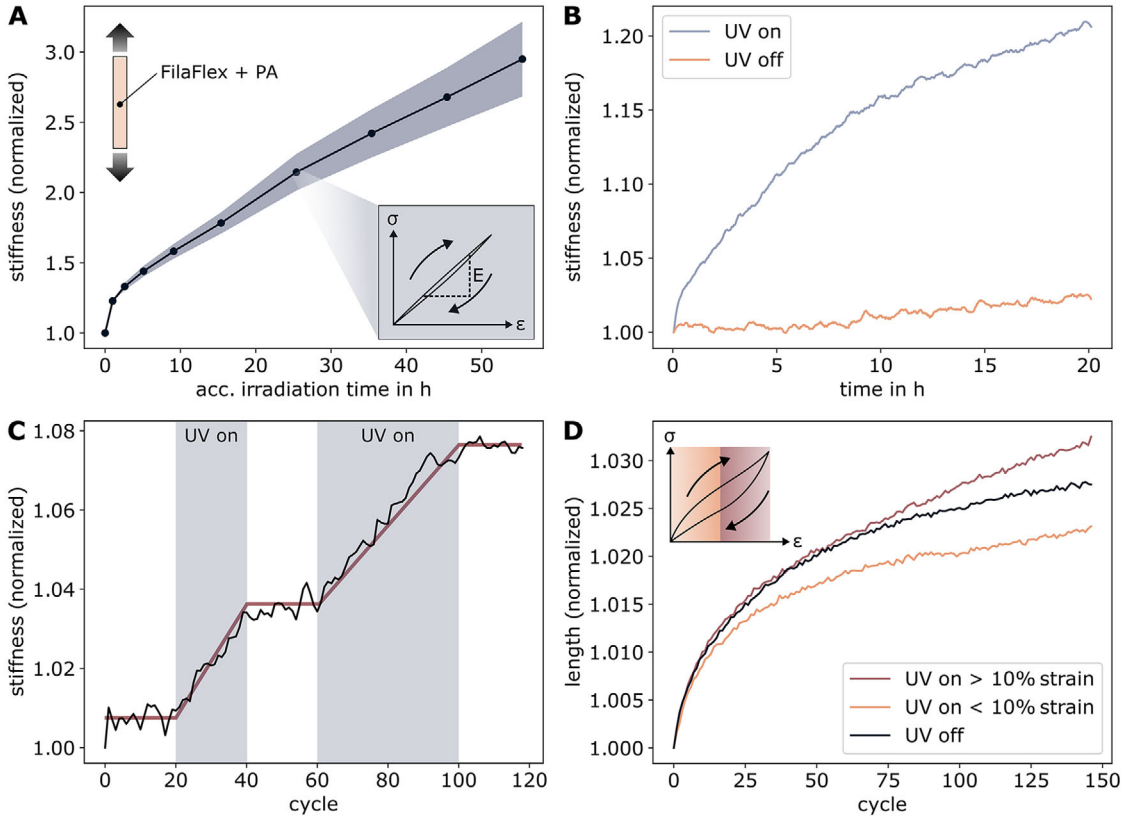


Figure 3. UV induced property changes of TPU + PA. A) Intermittent stiffness probing of single-side irradiated specimens in UV chamber. Insert: Assessment of Young's modulus from the stress-strain curve. Black line: mean, shaded area: standard deviation (n = 4). B) Tensile testing during irradiation with UV-lights turned on or off. C) Intermittent UV irradiation during tensile testing. UV on in shaded areas, red line as visual guidance. C: Assessment of specimen's length if irradiated at strains $\varepsilon < 10\%$, $\varepsilon > 10\%$ or UV off during cyclic loading to 20% strain.

Finally, we find the specimen's length to change according to its irradiated state during loading. We tested this by switching the UV-lights with respect to the applied strain. We loaded the tensile specimens up to 20% strain and varied the light switching, so we irradiate either during strains $\varepsilon < 10\%$ or $\varepsilon > 10\%$. We then compared it to a non-irradiated specimen for the same testing procedure. In Figure 3D we see a change in length of all specimens during testing. However, the specimen irradiated during strains $\varepsilon < 10\%$ is shortest and the specimen irradiated during strains $\varepsilon > 10\%$ is longest. From these results we can conclude, that irradiation also induces a change in the shape of the specimen. When irradiated in the strained state, the specimens tend to elongate compared with lights turned off. In turn, they tend to resist deformation more when irradiated in the relaxed state.

The ability to shift our material's properties by means of UV irradiation while being easily manufacturable is especially intriguing, because we can employ 3D printing to create complex structures. This sets our material system apart from other crosslinkable polymer systems, especially systems involving heat to trigger property changes. Kim and Lee[51] introduced a crosslinkable thermoplastic urethane which contains azide functional groups on the side chain. This allows a wide span of achievable mechanical properties, triggered by temperatures 80–120 °C. However, this temperature range prohibits extrusion based 3D printing, because the process involves printing temperatures exceeding 200 °C, effectively surpassing the activation temperature prematurely. Even lower activation temperatures of ca. 70 °C are achieved by trainable hydrogel systems.[52,53] Their inherently more complex manufacturing makes these systems harder to apply to metamaterial structures but are very intriguing because of their wide span of mechanical properties, as Nonoyama et al.[52] report a 1800× stiffness increase for their proposed material.

Our system yields a reduced but significant stiffening effect, which is especially interesting for metamaterial applications because of the locally controllable stiffening by irradiation. Here, instability driven mechanical metamaterials are especially intriguing. Bertoldi et al.[54] reported on such an instability-driven material with holes collapsing upon compression. During loading, as soon as a critical stress is reached, the holes collapse into an elliptic shape, resulting in an overall negative Poisson's ratio of the metamaterial. We utilized the metamaterial's sensitivity to its base-material's stiffness, to contrast the stiffness differences before and after irradiation (**Figure 4A**). We first tested the metamaterial under compression, where we displace its top with a crossbeam allowed to tilt about its center (Figure 4B). The metamaterial homogeneously deformed upon compression, indicated by the horizontal orientation of the crossbeam. Subsequently, we placed the block in a UV chamber at $\lambda = 365$ nm but covered the left half to prevent irradiation in this region. We retested the specimen and found the crossbar tilted upon compression. This

 © 2025 The Author(s). Advanced Materials Technologies published by Wiley-VCH GmbH

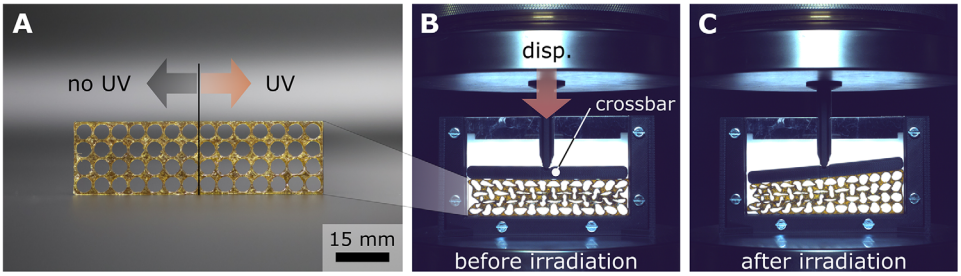


Figure 4. Metamaterial with instabilities. A) Unloaded, 3D printed specimen from TPU + PA. B) 4.5 mm compression of the specimen before irradiation. C) 4.5 mm compression of the specimen after 20 h irradiation of the right side: tilting indicates stiffness difference.

originates in the different stiffnesses in the left and right side, which is amplified by the instability-driven mechanism. The crossbar tilted toward the less stiff left side, as the metamaterial's holes collapsed there first (Figure 4C). This showcases a crucial benefit of the base-material: by targeted irradiation, local stiffness changes are achievable even after manufacturing of the structure. Especially intriguing is the fact, that we can control the stiffness of the region by the irradiation dose, potentially even allowing for graded material stiffness. This feature has the potential to become relevant for soft-robotics. Conrad and Teichmann et al.[55] have successfully 3D printed soft pneumatic logic and even a single input walking robot using the same TPU FilaFlex 70A base-material. Here, we would not only utilize 3D printing for manufacturing of complex hollow structures, but also tailor the stiffness locally afterwards. Locally stiffened structures can allow for increased load capacity or even change in behavior if the logic gates are treated. Furthermore, by locally changing the stiffness of the material, even switching of Poisson's ratio might be possible, dependent on a metamaterial's structure. Zhao et al.[56] report this ability for their multimaterial metamaterial, albeit for a globally increased temperature. Both approaches would result in 4D-printed systems, as Walker et al.[57] defined it, because an external, non mechanical stimulus yields a change in mechanical properties.

2.3. Harnessing Property Change for Training

The TPU + PA base-material gives us the potential to harness UV induced property changes in a trainable material system. For this, we employed a mechanical metamaterial with a distinct feature: switching lateral expansion upon vertical compression. As we described in a previous work,[36] we can tune the metamaterial's expansion behavior by its geometric features. Upon compression, the metamaterial initially exhibits lateral contraction, but when a critical deformation is reached, it starts expanding past its initial width: it effectively switches Poisson's ratio from negative to positive by closing internal gaps. By means of FFF 3D printing, we successfully manufactured the metamaterial as the core of the trainable material system. The metamaterial's arms can subsequently switch an optical light barrier (**Figure 5**A) in the test setup to trigger UV-irradiation upon compression (Figure 5B and 6A). Over the course of multiple compression cycles we expect the metamaterial's properties to change. Hence the fraction of the load-cycle with lights on alters due to the metamaterial's arms interacting with the optical light barrier. This is expected because of to the aforementioned characteristics of the base-material: modified shape and stiffening.

In Figure 6B,C, we clearly observe this behavior, derived from the material's crosslinking abilities. Here, only the metamaterial which employed PA and was subjected to UV irradiation showed an increased fraction of the load cycle with activated UV lights. In contrast, if unmodified TPU is used, or the UV-lights are turned off, we see a constant percentage of light-on time (Figure 6B,C). Because the testing was conducted using displacement controlled testing, we can assume that the change in light-on time is due to a shape change of the specimen: the metamaterial's internal gaps close immediately upon compression hence expansion (and therefore light-on time) happens during a larger fraction of the load-cycle.

This is further emphasized by the height of the specimen. While all specimens seem to conform to compression, only the specimen utilizing PA and UV changes its height significantly throughout the testing, as depicted in **Figure 7**A. This change in height is accompanied by a change of the specimen's stiffness. We see a sharp stiffness-increase for the metamaterial with PA and UV light, while the other specimens do not undergo a comparable stiffness increase (Figure 7B). This change in stiffness can be explained by two factors. First, the base-material becomes stiffer by UV activated crosslinking, similar to the results in Figure 3B. Second, the specimen's significant change in height results in closed internal gaps even upon unloading of the specimen. This results in an overall stiffer metamaterial compared

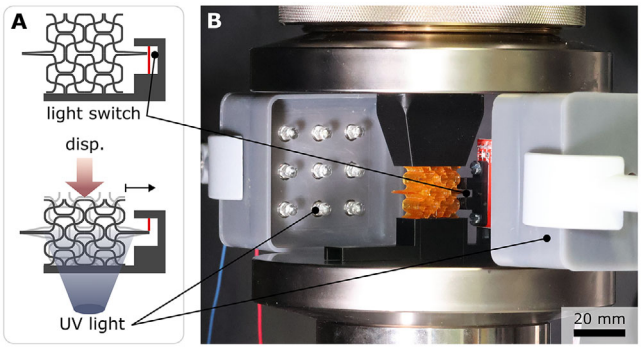


Figure 5. Test setup and working principle of the training process. A: The metamaterial is placed next to a light switch (top). Upon compression, the metamaterial expands and breaks the light switch, which triggers the UV lights. B: UV lights are placed front and rear of the specimen. The specimen is placed between the compression plates of the testing machine.

© 2025 The Author(s). Advanced Materials Technologies published by Wiley-VCH GmbH

2365709x, 2025, 23, Downloaded from https://advanced.onlinelibrary.wiley.com/doi/10.1002/admt.202501416 by Vyacheslav Slesarenko - Albert-Ludwigs-Universitat , Wiley Online Library on [04/11/2026]. See the Terms and Conditions (https://onlinelibrary.wiley.com/terms-and-conditions) on Wiley Online Library for rules of use; OA articles are governed by the applicable Creative Commons License

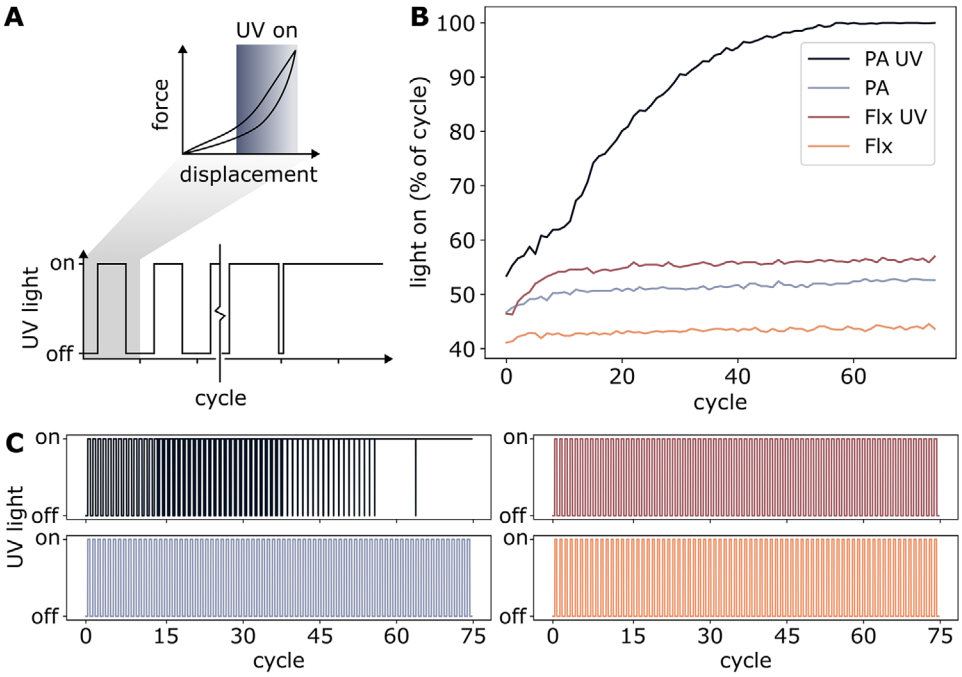


Figure 6. Displacement controlled training of the metamaterial system. A) The UV lights are activated by the metamaterial's expansion upon a specific displacement. This governs the percentage of light-on time during the testing cycle. B) Light-on percentage per test-cycle. PA with UV-lights activated saturates during testing. C) Light switching duty cycles per specimen and test. For clarity, switching times shorter than 10 s are not plotted.

to its initial state, independent of the base-material's property changes. In this case, the material adapts its height in order to keep the light on and gets a slightly deformed geometry.

Additionally, the metamaterial system allows for another mode of stimulus adaption. To independently assess the stiffening of the base-material, we designed a testing procedure comprised of two types of compression forces. The first compression force (F_{probe} = 1 N) was not sufficient to trigger the UV-lights by the metamaterial's lateral expansion (**Figure** 8A top). The compression was followed by 15 min uncompressed hold. After a repetition of the cycle, the second compression force followed. This force (F_{max} = 1.7 N) was sufficient to trigger a 15 min UV irradiation event (Figure 8A bottom). After 23 cycles we found the UV-lights not being triggered by F_{max} anymore. This originates form the base-material being sufficiently stiffened by UV-irradiation, resulting in a successfully trained metamaterial system, able to resist the compression force (Figure 8B,C).

The observed stiffening upon compression resembles adaptation or training mechanisms we find in nature. Muscles grow due to repeated weight training, ultimately they are able to lift a heavier weight.[1] Compared to that, our system becomes stiffer upon repeated compression, ultimately it is able to resist a higher force. Fitness enhancing properties of biological tissues have inspired works that similarly resemble training on a material level. Matsuda et al.[58] have introduced a hydrogel capable of "self-growing" upon a mechanical stimulus, resulting in a stretching induced stiffening. While the system elegantly trains upon the single mechanical stimulus, it relies on a hydrogel system, which limits its applicability and deployable environment. Pavlovian materials further elaborate on the aspect of training, were

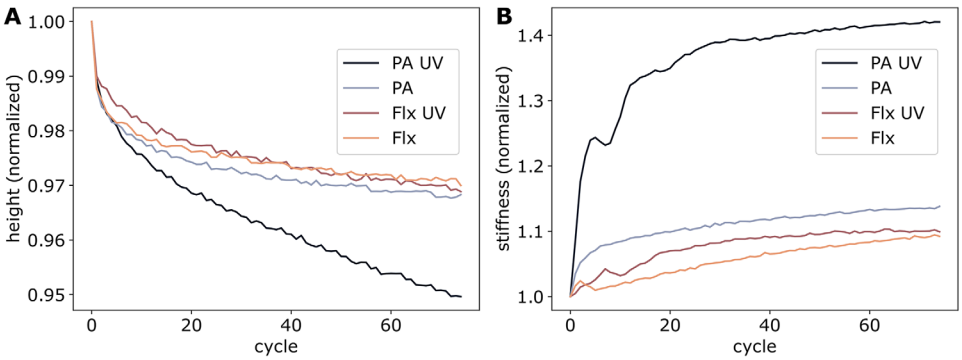


Figure 7. Mechanical evaluation of the metamaterial during testing. A) Height of the specimen (no mechanical load applied). B) Stiffness per metamaterial during cycled compression.

© 2025 The Author(s). Advanced Materials Technologies published by Wiley-VCH GmbH

2365709x, 2025, 23, Downloaded from https://advanced.onlinelibrary.wiley.com/doi/10.1002/admt.202501416 by Vyacheslav Slesarenko - Albert-Ludwigs-Universitat , Wiley Online Library on [04/11/2026]. See the Terms and Conditions (https://onlinelibrary.wiley.com/terms-and-conditions) on Wiley Online Library for rules of use; OA articles are governed by the applicable Creative Commons License

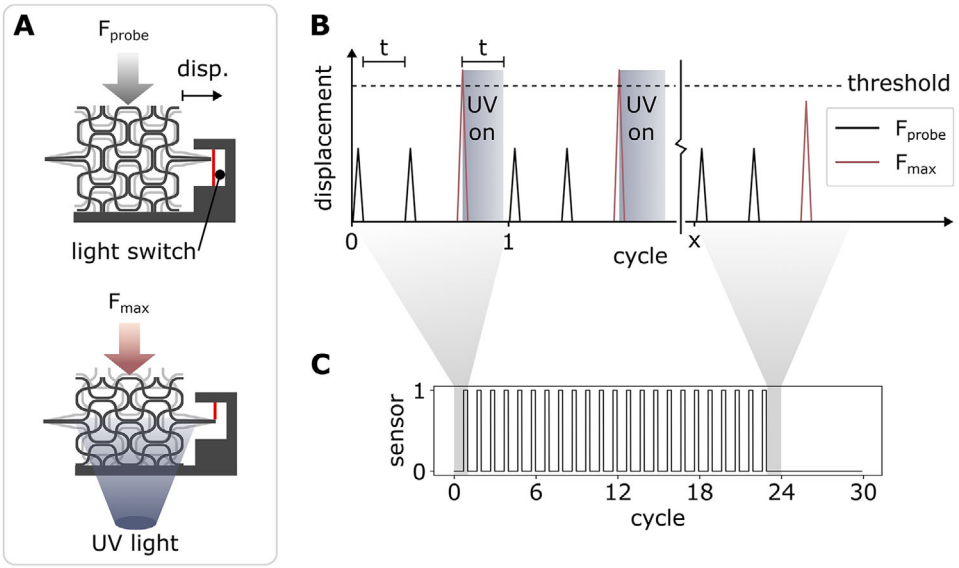


Figure 8. Threshold training. A) Top: F_{probe} is not sufficient to trigger the light by lateral expansion. Bottom: F_{max} triggers UV-lights by activating the light-switch. B) Testing procedure: F_{probe}, t = 15 min wait, F_{probe}, wait (t), F_{max}, wait (t). After x-cycles, the metamaterial is sufficiently stiff to resist F_{max}. C) Results from the test show no UV activation after about x = 23 testing-cycles.

the conjunction of two stimuli allow for a seemingly more intelligent system, capable of information processing, surpassing the sole reaction to mechanical loading.[59,60]

Here, we combine both abilities in one system: stiffening as reaction to a mechanical stimulus, facilitated by a secondary UV-stimulus. Furthermore, we open up the possibility to manufacture more complex geometries by means of 3D printing, effectively overcoming the limitations of previously discussed hydrogel-systems. This means that the metamaterial comprised of TPU + PA can achieve two types of behavior: it can be directly stiffened by an external UV-stimulus or its complex deformation can be harnessed in a system with sensors to make it adaptable or trainable toward mechanical loading.

3. Conclusion

Stimuli-responsive materials are crucial for the development of trainable systems, exhibiting life-like behavior. Here we present a 3D printable TPU at the core of a material system capable of adapting to a mechanical stimulus. We successfully incorporated CHic-able groups into 3D printable TPU filament, fabricated tensile specimens and mechanical metamaterials to assess and showcase its capabilities. By testing tensile specimens, we showed an up to 300% increase in stiffness upon irradiation. The changes in stiffness are rapid and can be introduced in an intermittent manner, carefully tailoring the specimens stiffness by accumulating stiffness. The change in stiffness is also accompanied by a change in the specimen's dimensions, if the specimen is irradiated in a deformed state. Additionally, we show the local effects of the irradiation driven crosslinking by harnessing an instability driven metamaterial with holes. We clearly see, that irradiation of one half leads to a collapse of the structure's other half under compression. Tilting of the specimen's top surface clearly indicates locally higher base-material stiffness.

Finally, we utilized both change in dimensions and change in stiffness to create a trainable material system, with a 3D printed metamaterial at its core. Upon compression, the specimen activates its own UV irradiation by means of a geometrically designed point of expansion. After a sufficient number of loading cycles the material becomes adapted to the compression and shows an increased stiffness. Furthermore, we employed the metamaterial's tailored point of expansion to create a system capable of threshold sensitive training. Only if the applied force results in a minimum expansion, the UV irradiation is turned on. We could successfully show that initially the applied force was large enough to trigger the light source, but eventually the metamaterial's increased stiffness prohibited the triggering event. This can be interpreted as the material system training to resist the triggering force.

The metamaterial comprised of TPU + PA can achieve two types of behavior. It can be directly stiffened by an external UV-stimulus or its complex deformation can be harnessed in a system with sensors to make it trainable toward mechanical loading. The observed stimulus stiffening of our complex 3D printed objects resembles adaptation or training mechanisms we find in nature, like growing muscles due to repeated training. The developed fitness enhancing properties on a material level closely resemble these biological tissues. The here described material system has the potential to improve soft robotics by locally tuning material properties after manufacturing, but it can also be deployed in other trainable materials leading to life-like, stimuli-responsive systems.

4. Experimental Section

Synthesis—Synthesis of Compound 1: In a dried three-neck-round-bottom flask equipped with magnetic stirring bar, a solution of Ethylene glycol (16.43 mL, 293.8 mmol, 4.00 eq) and

© 2025 The Author(s). Advanced Materials Technologies published by Wiley-VCH GmbH

2365709x, 2025, 23, Downloaded from https://advanced.onlinelibrary.wiley.com/doi/10.1002/admt.202501416 by Vyacheslav Slesarenko - Albert-Ludwigs-Universitat , Wiley Online Library on [04/11/2026]. See the Terms and Conditions (https://onlinelibrary.wiley.com/terms-and-conditions) on Wiley Online Library for rules of use; OA articles are governed by the applicable Creative Commons License

4-dimethylaminopyridine (2.96 g, 24.24 mmol, 0.33 eq) in acetonitrile (100 mL) was prepared under nitrogen and cooled to 0 °C. 1-Ethyl-3-(3-dimethylaminopropyl)carbodiimide hydrochloride (9.32 g, 48.62 mmol, 1.10 eq) was then added slowly. Phenyl acetic acid (15.49 g, 80.79 mmol, 1.00 eq) was dissolved in acetonitrile (100 mL) and added dropwise to the above mentioned solution. The reaction mixture was stirred at 0 °C for 1 h.

The reaction was then stopped with water (150 mL). The aqueous phase was then extracted thrice with ethyl acetate (3 times 100 mL). The organic phases were then combined, dried over Na_2SO_4 and the solvent was removed under reduced pressure. 12.75 g of Compound 1 was obtained as a liquid (96%).

^{1}H NMR (250 MHz, Chloroform-d) δ 7.43 – 7.23 (m, 5H), 4.31 (s, 1H), 4.23 (t, J = 4.7 Hz, 2H), 3.80 (t, J = 5.6 Hz, 2H), 3.68 (d, J = 2.2 Hz, 2H). ^{13}C NMR (63 MHz, CDCl3) δ 172.05, 147.73, 127.24, 78.81, 77.24, 75.66, 41.25.

Synthesis—Synthesis of Compound 2: In a 500 mL three-necked flask with septum, 2-hydroxyantraquinone (5.47 g, 24.42 mmol, 1.1 eq) was dissolved in tetrahydrofuran (200 mL) under nitrogen. Then triphenylphosphine (17.47 g, 66.59 mmol, 3 eq) and diethyl azodicarboxylate (11.26 mL, 66.59 mmol, 3.00 eq) were added and the reaction mixture was stirred for 1 h at room temperature. Compound 1 (4 g, 22.2 mmol, 1 eq) was then added in tetrahydrofuran (50 mL) and the reaction solution was stirred overnight at room temperature.

The reaction was then stopped with water (150 mL). The aqueous phase is then extracted thrice with ethyl acetate (3 times 100 mL). The organic phases are then combined, dried over Na_2SO_4 and the solvent was removed under reduced pressure.

The crude product was then purified by silica gel column chromatography (eluant Hexane/Ethyl acetate: 60/40) to afford 7.16 g of Compound 2 as a yellow solid was obtained (83%).

^{1}H NMR (250 MHz, Chloroform-d) δ 8.47 – 8.16 (m, 4H), 8.01 – 7.61 (m, 3H), 7.46 – 7.05 (m, 5H), 4.57 (t, J = 3.1, 2.5 Hz, 2H), 4.42 (t, J = 3.1, 2.5 Hz, 2H), 3.73 (s, 2H). ^{13}C NMR (63 MHz, CDCl3) δ 150.29, 140.34, 134.27, 133.80, 133.65, 129.87, 129.28, 128.67, 127.23, 124.53, 123.81, 121.60, 110.57, 66.50, 62.76, 41.22

Synthesis—Synthesis of PA: In a brown, dried three-neck-round-bottom flask equipped with magnetic stirring bar, a solution of compound 2 (2 g, 5.18 mmol, 1.00 eq) in acetonitrile (20 mL) was prepared under nitrogen and cooled to 0 °C. 4-Acetamidobenzenesulfonyl azide (1.52 g, 6.31 mmol, 1.22 eq) was added and the reaction mixture was degassed under argon bubbling for 15 min. 1,8-Diazabicyclo[5.4.0]undec-7-ene (1.55 mL, 10.35 mmol, 2.00 eq) was added at 0 °C and the solution was allowed to warm up to room temperature. The reaction mixture was stirred overnight.

The reaction was then stopped with water (150 mL). The aqueous phase is then extracted thrice with ethyl acetate (3 times 100 mL). The organic phases are then combined, dried over Na_2SO_4 and the solvent was removed under reduced pressure.

The crude product was then purified by silica gel column chromatography (eluant Hexane/Ethyl acetate: 80/20) to afford 4.16 g of PA were obtained as a yellow solid (78% yield).

^{1}H NMR (250 MHz, Chloroform-d) δ 8.34 (td, J = 6.5, 6.1, 3.3 Hz, 3H), 7.89 – 7.76 (m, 3H), 7.52 (d, J = 7.8 Hz, 2H), 7.48 – 7.28 (m, 3H), 7.23 (t, J = 7.1 Hz, 1H), 4.74 (t, J = 4.4 Hz, 2H), 4.50 (t, J = 4.4 Hz, 2H). ^{13}C NMR (63 MHz, CDCl3) δ 163.21, 142.18, 134.29, 133.80, 133.55, 129.87, 128.93, 127.14, 124.06, 121.51, 119.46, 110.62, 78.69, 77.11, 75.52, 50.35. UV-Vis (DCM, 2.10^{-5} mol L^{-1}): $\varepsilon_{265\ nm}$ = 31,000 L mol^{-1} cm^{-1}; $\varepsilon_{330\ nm}$ = 2,500 L mol^{-1} cm^{-1}; $\varepsilon_{365\ nm}$ = 1,900 L mol^{-1} cm^{-1}; $\varepsilon_{400\ nm}$ = 587 L mol^{-1} cm^{-1}.

Synthesis—Filament modification: 9.86 g of filament was immersed in 197 mL of a 5 mg mL^{-1} solution of PA in dichloromethane (DCM) (986 mg of PA in 197 mL of DCM). The solution was then agitated until the filament absorbed the whole solution by swelling. The filament was then dried at room temperature for 1 h before being heated at 100 °C for 18 h.

To quantify the inserted crosslinker, the modified filament was melted and spread on a glass slide until the layer is 0.07 mm thick. The layer was then analysed with a UV-Vis spectrometer (Agilent, Cary 60) and compared to a similar layer of Filaflex 70A (**Figure 9**). The absorbtion of Filaflex was null at 400 nm while the modified filament exhibit an absorption of 0.513. Using the Beer-Lambert law, 5 wt% of the crosslinker was obtained in the final filament.

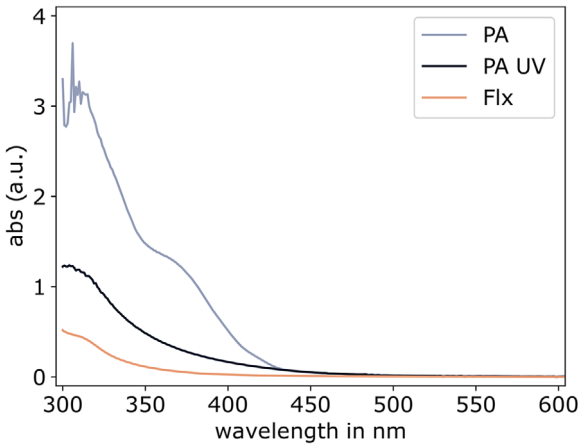


Figure 9. UV-Vis spectrum of FilaFlex TPU, FilaFlex + PA and FilaFlex + PA after irradiation at 365 nm for 1 h (solid state, 0.07 mm thickness).

To demonstrate the crosslinking spectroscopically, a layer of PA-containing filament was irradiated for 1 h at 365 nm. After this time, the absorption band around 365 nm disappears. The absorption around 300 nm was also reduced but remains higher than that of the pure filament, thus providing UV protection.

Printing: The filament was subsequently used to print the specimens for testing. We printed with standard and PA modified transparent Filaflex 70A TPU (Recreus, Alicante, Spain) with 0.4 mm nozzle on a standard Prusa MK4 3D printer (Prusa, Prague, Czech Republic). The chosen printing settings were as follows: print temperature = 220 °C, bed temperature = 60 °C, layer height = 0.1 mm (initial layer height = 0.2 mm), print speed = 10 mm s^{-1}, infill = 100% and "avoid crossing perimeters" activated. Tensile specimens were printed in a single layer with following dimensions: 0.2 × 4 × 40 mm (**Figure 10A**). The metamaterial specimens consist of 2 × 2 unit cells with 5 mm arms (Figure 10B), internal dimensions are specified in Figure 10C.

Tensile Testing: The tensile test results depicted in Figure 3 were conducted on a universal testing machine (ZwickRoell, Ulm, Germany) equipped with a 500 N load cell. For all testing depicted in Figure 3A, 4 specimens were each tested 10 times to a displacement of 2 mm at a testing speed of 4 mm min^{-1}. The obtained force-displacement data was converted to stress-strain and Young's modulus was evaluated in the region of 80-100% of the load cycle. The average of 4 central cycles was used per specimen, mean ± standard deviation was calculated across the tested specimens. Subsequently, the specimens were placed on electrical tape (to ensure one-sided irradiation) and irradiated in the UV-chamber Bio-Link 365 (Vilber, Marne La Vallée, France). Irradiation time was determined by Renard R5 series, meaning the irradiation cycles lasted: 1 h, 1.6 h, 2.5 h, 4 h, 6.3 h and 4 × 10 h.

Tensile tests shown in Figure 3B employed a tensile specimen with FilaFlex 70A + PA per curve. However, here two UV lamps were used during tensile testing, one placed in front and one behind the specimen. We used custom lamps, which were comprised of 3 × 3 arrays of LEDs (λ = 365–375 nm) (Figure 5B). The same setup was used for intermittent irradiation in Figure 3C, with the lamps only switched on for 20 min after 20 cycles and for 40 min after 60 cycles.

To test the specimen's length dependent on the irradiated state, the aforementioned setup was modified. Here, it was tested 150 times to a displacement of 5 mm (20% strain) at a testing speed of 10 mm min^{-1}. We tested three specimens, one with UV lights off, one with UV activated for displacements < 2.5 mm and another one with UV activated for displacements > 2.5 mm. To accomplish this in a repeatable way, we tracked the testing machine's cross-head with a laser distance sensor (Baumer OADK

© 2025 The Author(s). Advanced Materials Technologies published by Wiley-VCH GmbH

2365709x, 2025, 23, Downloaded from https://advanced.onlinelibrary.wiley.com/doi/10.1002/admt.202501416 by Viacheslav Slesarenko - Albert-Ludwigs-Universitat , Wiley Online Library on [04/11/2026]. See the Terms and Conditions (https://onlinelibrary.wiley.com/terms-and-conditions) on Wiley Online Library for rules of use; OA articles are governed by the applicable Creative Commons License

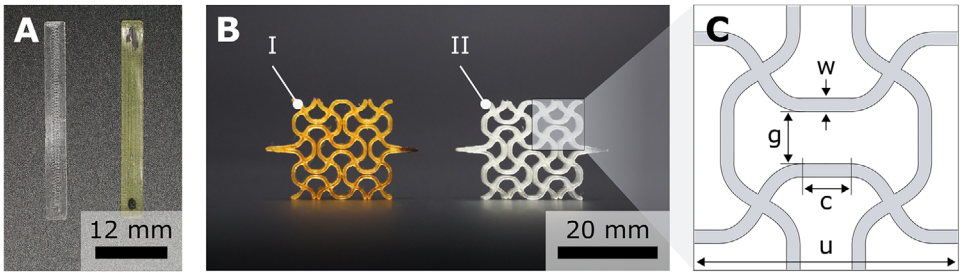


Figure 10. A) Tensile specimens with dimensions 0.2 × 4 × 40 mm. Left: transparent FilaFlex 70A, right: Filaflex 70A + PA. B) Printed metamaterials, with a thickness of 10 mm. I: Filaflex 70A + PA, II: Unmodified, transparent FilaFlex 70A. C) Size of unit cell u = 10 mm, gap size g = 0.5 mm, contact length c = 0.45 mm, beam width w = 0.4 mm.

2517480/S14C, Frauenfeld, Switzerland) and switched the UV-lamps automatically with a relay and a microcontroller (sparkfun Artemis, Niwot, USA). The specimen's length was determined at the end of each load cycle, when returned to the preload force of 0.05 N. This made sure, the specimen was flat and not buckled out of plane.

Compression Testing of Metamaterial with Holes: The metamaterial with holes resembled the shape proposed by Bertoldi et al.[54] The holes had a diameter of 4.6 mm and a wall thickness of 0.6 mm between them, forming the metamaterial block with a thickness of 1.5 mm in a 4 × 14 array (Figure 4A). They were printed on the aforementioned Prusa 3D printer from FilaFlex 70A + PA. Subsequently, the metamaterial was placed in the test-setup. The test-setup was comprised of two clear plexiglas-windows, preventing out of plane buckling, a crossbar for even load application and a compression-pin (Figure 4B). The compression pin was pushed in 6 mm at 18 mm min^{-1} by the ZwickRoell universal testing machine. After this initial testing, the left half of the specimen was covered in aluminum foil and then placed in the Bio-Link 365 UV chamber for 10 h for irradiation from the top. The specimen was then flipped and irradiated for another 10 h from the bottom. Finally, the specimen is retested in the compression setup, were the notched crossbar allowed for rotation and therefore visualization of the different stiffnesses across the specimen.

Compression Testing of Metamaterial with Arms: For compression testing of the metamaterial with arms, the setup displayed in Figure 5 was used. Four metamaterials were tested with arms, as depicted in Figure 10. They were placed on a 3D printed fixture with central needles to mitigate lateral movement and an optical end-switch. The end-switch was triggered by the specimen's arm, reaching into its optical pathway upon sufficient compression due to lateral expansion. The light-switch was connected to an Arduino uno microcontroller (Monza, Italy). The microcontroller subsequently switched on the UV lights by a relay upon detected expansion. It was tested with the same universal testing machine, equipped with the aforementioned 500 N load cell up to a compression of 5 mm at a testing speed of 5 mm min^{-1}. The testing was recorded with a synchronized CMOS camera (IDS UI-3880CP, Imaging Development Systems, Obersulm, Germany) and the end-switch data was logged. The testing was done with UV lights connected or disconnected from power per tested material, as described in **Table 1**.

For force controlled threshold testing, a single metamaterial printed from FilaFlex 70A + PA was used. The setup remained similar to the aforementioned, with a difference in the testing procedure, comprised of three steps: First, the metamaterial was compressed to F_{probe} = 1 N at a testing speed of 3 mm min^{-1} followed by a t = 15 min pause, this was repeated a second time. Third, the metamaterial was compressed to F_{max} = 1.7 N, followed by another pause of duration t (Figure 8). The third loading had the aim of triggering the optical end-switch, after which the UV lights were turned on for 15 min, facilitated by the Arduino microcontroller. The testing was repeated 30 times with the goal of reaching sufficient resistance of the metamaterial against the applied force, so the lights would not be turned on.

Table 1. Metamaterials with their material composition and testing condition.

Material	Testing condition
FilaFlex 70A	no UV
FilaFlex 70A	UV
FilaFlex 70A + PA	no UV
FilaFlex 70A + PA	UV

Acknowledgements

This research was funded by the Deutsche Forschungsgemeinschaft (DFG, German Research Foundation) under Germany's Excellence Strategy: EXC-2193/1-390951807.

Open access funding enabled and organized by Projekt DEAL.

Conflict of Interest

The authors declare no conflict of interest.

Author Contributions

D.S. and J.L. contributed equally to the work. J.L. synthesized the crosslinker and prepared the filament. D.S. designed, printed, tested and evaluated the specimens and built the training system. V.S. and J.L. conceived and supervised the research. J.R. advised and helped with the conceptualization of the experiments. D.S. and J.L. wrote the original draft. All authors discussed the results and wrote the manuscript. All authors reviewed the manuscript.

Data Availability Statement

The data that support the findings of this study are available from the corresponding author upon reasonable request.

Keywords

C,H-insertion crosslinking, materials training, mechanical metamaterial, stimuli responsive

Received: July 3, 2025
Revised: September 12, 2025
Published online: October 17, 2025

© 2025 The Author(s). Advanced Materials Technologies published by Wiley-VCH GmbH

2365709x, 2025, 23, Downloaded from https://advanced.onlinelibrary.wiley.com/doi/10.1002/admt.202501416 by Vyacheslav Slesarenko - Albert-Ludwigs-Universitat , Wiley Online Library on [04/11/2026]. See the Terms and Conditions (https://onlinelibrary.wiley.com/terms-and-conditions) on Wiley Online Library for rules of use; OA articles are governed by the applicable Creative Commons License

[1] D. C. Hughes, S. Ellefsen, K. Baar, *Cold Spring Harbor Perspect. Med.* **2017**, *8*, a029769.
[2] P. D. Chilibeck, D. G. Sale, C. E. Webber, *Sports Medicine* **1995**, *19*, 103.
[3] P. Fratzl, *J. R. Soc., Interface* **2007**, *4*, 637.
[4] N. P. R. Anten, R. Alcalá-Herrera, F. Schieving, Y. Onoda, *New Phytologist* **2010**, *188*, 554.
[5] K. Otsuka, X. Ren, *Intermetallics* **1999**, *7*, 511.
[6] A. Amadi, M. Mohyaldinn, S. Ridha, V. Ola, *J. Alloys Compd.* **2024**, *976*, 173227.
[7] H. E. Meijer, L. E. Govaert, *Prog. Polym. Sci.* **2005**, *30*, 915.
[8] C. Ni, D. Chen, Y. Yin, X. Wen, X. Chen, C. Yang, G. Chen, Z. Sun, J. Wen, Y. Jiao, C. Wang, N. Wang, X. Kong, S. Deng, Y. Shen, R. Xiao, X. Jin, J. Li, X. Kong, Q. Zhao, T. Xie, *Nature* **2023**, *622*, 748.
[9] E. M. Terentjev, *J. Phys.: Condens. Matter* **1999**, *11*, R239.
[10] M. Chen, M. Gao, L. Bai, H. Zheng, H. J. Qi, K. Zhou, *Adv. Mater.* **2023**, *35*, 23.
[11] Y. S. Zhang, A. Khademhosseini, *Science* **2017**, *356*, 6337.
[12] O. Skarsetz, V. Slesarenko, A. Walther, *Adv. Sci.* **2022**, *9*, 2201867.
[13] O. Skarsetz, P. J. Swinkels, J. Figueiredo da Silva, G. Vozzolo, M. Masukawa, G. Fusi, B. Dúzs, Y. Lassiat, C. Drees, V. Slesarenko, A. Walther, *Adv. Mater.* **2025**.
[14] W. Pu, F. Wei, L. Yao, S. Xie, *J. Mater. Sci.* **2022**, *57*, 12202.
[15] J. Wang, F. Jin, X. Dong, J. Liu, M. Zheng, *Adv. Mater. Technol.* **2022**, *7*, 8.
[16] A. Tabatabaeian, S. Liu, P. Harrison, E. Schlangen, M. Fotouhi, *Composites, Part A* **2022**, *163*, 107236.
[17] C. M. Geiselhart, H. Mutlu, C. Barner-Kowollik, *Angew. Chem., Int. Ed.* **2021**, *60*, 17290.
[18] D. Schwarz, V. Slesarenko, *Composites Part C: Open Access* **2025**, 100586.
[19] P. Testa, R. W. Style, J. Cui, C. Donnelly, E. Borisova, P. M. Derlet, E. R. Dufresne, L. J. Heyderman, *Adv. Mater.* **2019**, *31*, 29.
[20] O. Skarsetz, R. Mathes, R. S. Schmidt, M. Simon, V. Slesarenko, A. Walther, *ACS Appl. Mater. Interfaces* **2024**, *16*, 38511.
[21] T. Mai, T. Yasui, R. Tanaka, H. Masunaga, T. Kabe, K. Tsunoda, S. Sakurai, K. Urayama, *Adv. Sci.* **2024**, *11*, 12.
[22] J. Diani, B. Fayolle, P. Gilormini, *Eur. Polym. J.* **2009**, *45*, 601.
[23] T. Chen, M. Pauly, P. M. Reis, *Nature* **2021**, *589*, 386.
[24] A. A. Zadpoor, *Mater. Horiz.* **2016**, *3*, 371.
[25] K. Che, C. Yuan, J. Wu, H. Jerry Qi, J. Meaud, *J. Appl. Mech.* **2016**, *84*, 1.
[26] M. Kadic, T. Bückmann, R. Schittny, P. Gumbsch, M. Wegener, *Phys. Rev. Appl.* **2014**, *2*, 054007.
[27] T. Frenzel, M. Kadic, M. Wegener, *Science* **2017**, *358*, 1072.
[28] X. Fang, D. Yu, J. Wen, Y. Dai, M. R. Begley, H. Gao, P. Gumbsch, *Nature* **2025**.
[29] H. M. A. Kolken, A. A. Zadpoor, *RSC Adv.* **2017**, *7*, 5111.
[30] R. Gatt, M. Vella Wood, A. Gatt, F. Zarb, C. Formosa, K. M. Azzopardi, A. Casha, T. P. Agius, P. Schembri-Wismayer, L. Attard, N. Chockalingam, J. N. Grima, *Acta Biomater.* **2015**, *24*, 201.
[31] J. U. Surjadi, L. Gao, H. Du, X. Li, X. Xiong, N. X. Fang, Y. Lu, *Adv. Eng. Mater.* **2019**, *21*, 3.
[32] J. Valente, E. Plum, I. J. Youngs, N. I. Zheludev, *Adv. Mater.* **2016**, *28*, 5176.
[33] K. K. Dudek, J. A. I. Martínez, G. Ulliac, M. Kadic, *Adv. Mater.* **2022**, *34*, 14.
[34] M. Miniaci, A. Krushynska, F. Bosia, N. M. Pugno, *New J. Phys.* **2016**, *18*, 083041.
[35] T.-C. Lim, *Oxford Open Materials Science* **2022**, *2*, 1.
[36] D. Schwarz, G. Felsch, F. Tauber, S. Schiller, V. Slesarenko, *Mater. Des.* **2023**, *236*, 112468.
[37] P. Jiao, J. Mueller, J. R. Raney, X. Zheng, A. H. Alavi, *Nat. Commun.* **2023**, *14*, 1.
[38] J. Kost, A. Bleiziffer, D. Rusitov, J. Rühe, *J. Am. Chem. Soc.* **2021**, *143*, 10108.
[39] M. Liu, C. Xu, H. Zhao, T. Jiang, S. Chen, J. Xuan, *Adv. Funct. Mater.* **2025**.
[40] R. Toomey, D. Freidank, J. Rühe, *Macromolecules* **2004**, *37*, 882.
[41] D. Rusitov, F. Deussen, J. Rühe, *Adv. Mater. Interfaces* **2023**, *10*, 26.
[42] P. F. Kotrade, J. Rühe, *Angew. Chem., Int. Ed.* **2017**, *56*, 14405.
[43] T. A. Weber, L. Metzler, P. L. Fosso Tene, T. Brandstetter, J. Rühe, *ACS Appl. Mater. Interfaces* **2022**, *14*, 25147.
[44] M. Akiba, *Prog. Polym. Sci.* **1997**, *22*, 475.
[45] Q. Guo, *Thermosets Structure Properties And Applications*, Woodhead Publishing **2012**.
[46] J. Liotier, T. Piock, J. Rühe, *Macromolecules* **2024**, *58*, 1859.
[47] A. J. Straub, F. D. Scherag, H. I. Kim, M.-S. Steiner, T. Brandstetter, J. Rühe, *Langmuir* **2021**, *37*, 6510.
[48] T. Kanokwijitsilp, M. Körner, O. Prucker, A. Anton, J. Lübke, J. Rühe, *Macromolecules* **2021**, *54*, 6238.
[49] A. Boubakri, N. Guermazi, K. Elleuch, H. Ayedi, *Mater. Sci. Eng., A* **2010**, *527*, 1649.
[50] L. Rosu, C. Cascaval, C. Ciobanu, D. Rosu, E. Ion, C. Morosanu, M. Enachescu, *J. Photochemistry Photobiology A: Chemistry* **2005**, *169*, 177.
[51] H. Kim, K. J. Lee, *Polymer* **2021**, *236*, 124350.
[52] T. Nonoyama, Y. W. Lee, K. Ota, K. Fujioka, W. Hong, J. P. Gong, *Adv. Mater.* **2019**, *32*, 4.
[53] S. Hu, Y. Fang, C. Liang, M. Turunen, O. Ikkala, H. Zhang, *Nat. Commun.* **2023**, *14*, 1.
[54] K. Bertoldi, P. M. Reis, S. Willshaw, T. Mullin, *Adv. Mater.* **2010**, *22*, 361.
[55] S. Conrad, J. Teichmann, P. Auth, N. Knorr, K. Ulrich, D. Bellin, T. Speck, F. J. Tauber, *Sci. Rob.* **2024**, *9*, 86.
[56] Z. Zhao, C. Yuan, M. Lei, L. Yang, Q. Zhang, H. Chen, H. J. Qi, D. Fang, *Phys. Rev. Appl.* **2019**, *11*, 044074.
[57] A. Walker, K. Shea, *Smart Mater. Struct.* **2024**, *33*, 115047.
[58] T. Matsuda, R. Kawakami, R. Namba, T. Nakajima, J. P. Gong, *Science* **2019**, *363*, 504.
[59] H. Zhang, H. Zeng, A. Priimagi, O. Ikkala, *Adv. Mater.* **2020**, *32*, 20.
[60] H. Zeng, H. Zhang, O. Ikkala, A. Priimagi, *Matter* **2020**, *2*, 194.

© 2025 The Author(s). Advanced Materials Technologies published by Wiley-VCH GmbH

2365709x, 2025, 23, Downloaded from https://advanced.onlinelibrary.wiley.com/doi/10.1002/admt.202501416 by Viacheslav Slesarenko - Albert-Ludwigs-Universitat , Wiley Online Library on [04/11/2026]. See the Terms and Conditions (https://onlinelibrary.wiley.com/terms-and-conditions) on Wiley Online Library for rules of use; OA articles are governed by the applicable Creative Commons License